

Modeling three-dimensional network formation with an atomic lattice model: Application to silicic acid polymerization

Lin Jin, Scott M. Auerbach,^{a)} and Peter A. Monson^{b)}

Department of Chemical Engineering and Department of Chemistry, University of Massachusetts, Amherst, Massachusetts 01003, USA

(Received 21 December 2010; accepted 15 March 2011; published online 7 April 2011)

We present an atomic lattice model for studying the polymerization of silicic acid in sol-gel and related processes for synthesizing silica materials. Our model is based on Si and O atoms occupying the sites of a body-centered-cubic lattice, with all atoms arranged in SiO₄ tetrahedra. This is the simplest model that allows for variation in the Si–O–Si angle, which is largely responsible for the versatility in silica polymorphs. The model describes the assembly of polymerized silica structures starting from a solution of silicic acid in water at a given concentration and pH. This model can simulate related materials—chalcogenides and clays—by assigning energy penalties to particular ring geometries in the polymerized structures. The simplicity of this approach makes it possible to study the polymerization process to higher degrees of polymerization and larger system sizes than has been possible with previous atomistic models. We have performed Monte Carlo simulations of the model at two concentrations: a low density state similar to that used in the clear solution synthesis of silicalite-1, and a high density state relevant to experiments on silica gel synthesis. For the high concentration system where there are NMR data on the temporal evolution of the Q_n distribution, we find that the model gives good agreement with the experimental data. The model captures the basic mechanism of silica polymerization and provides quantitative structural predictions on ring-size distributions in good agreement with x-ray and neutron diffraction data. © 2011 American Institute of Physics. [doi:10.1063/1.3575188]

I. INTRODUCTION

Sol-gel processing of silica has been studied extensively for over a century, reflecting its importance in materials science and ceramic engineering.^{1–4} Such sol-gel processing can yield nanoporous crystalline zeolites,⁵ mesoporous silica, such as MCM-41,⁶ and amorphous silica in monoliths, films, fibers, and monosized powders.^{7–9} Understanding structure formation from atomic to materials length scales is crucial for tailoring these materials for advanced applications in, e.g., catalysis and separations.¹⁰ Despite progress in experimental characterization,^{11–14} we still lack detailed information about the spatial structure of silica during its polymerization process. Molecular modeling has the potential to shed light on this, but is hampered by the complicated interplay of chemical and physical interactions at many length scales.¹⁵ To address this difficulty, we have developed a variety of models to capture the evolution of structure during silica polymerization.^{16–19} In this work we report on a new, atomic lattice model that captures many structural aspects of silica formation while allowing the study of very long lengths and times.

In previous work we reported a coarse-grained lattice model of nanoparticle growth in the clear solution synthesis of silicalite-1 (MFI).¹⁸ The body-centered-cubic (bcc) lattice was chosen because it is composed of two interpenetrating tetrahedral sublattices, and as such can represent the

tetrahedral structure of silica on one sublattice, while leaving lattice sites left over on the other sublattice to represent pore spaces. This model involves SiO₄ tetrahedra represented as particles on a body-centered-cubic lattice with second-neighbor repulsions, to generate a four-coordinate network that mimics the tetrahedral structure of silica. Although this lattice model allows the study of penetration of organic templates into the cores of nanoparticles—a process thought to be important for zeolite formation—the model leaves many structural questions unanswered because of the constraints imposed by coarse-graining. In particular, only one Si–O–Si angle (180°) is allowed in this model and only six-rings (rings containing six Si and six O atoms in alternation) can arise. In contrast, silica structures exhibit a wide range of Si–O–Si angles (130°–180°),²⁰ giving rise to primitive (irreducible) rings ranging from 3-rings up to 14-rings.^{21,22} While off-lattice models provide such flexibility,¹⁹ they can treat only relatively small system sizes.¹⁵ As such, the development of new lattice models that provide structural flexibility is of paramount importance. This can be achieved by adopting a more intricate lattice, by treating more complex interactions,^{23,24} or by resolving more detailed atomic structure. In the present work, we pursue this last approach tailored specifically to silica formation.

Silica polymerization can be written in the generic form,



It is widely believed that solution pH plays a significant role in this polymerization by controlling surface charges on

^{a)}Electronic mail: auerbach@chem.umass.edu.

^{b)}Electronic mail: monson@ecs.umass.edu.

silica particles. A pH of around 2 ± 0.5 is the isoelectric point of silica, where there is negligible net surface charge on silica particles.²⁵ Under such conditions, silicic acid monomers polymerize to form discrete particles before aggregation and gelation, and condensation kinetics is slow enough for experiments to follow and characterize. For example, Devreux *et al.*¹² studied the condensation kinetics by ²⁹Si NMR of a system containing tetra-ethoxysilane [Si(OC₂H₅)₄ or TEOS] using acidic conditions and excess water. (Low pH and high water-to-alkoxide ratio yields rapid and nearly complete hydrolysis of TEOS.) The NMR permits the determination of the Q_n distribution, where Q_n is the fraction of silicon atoms in the system that are connected to n bridging oxygen atoms.¹³ These data (*vide infra*) indicate that at the isoelectric point, room temperature silica condensation is very slow, requiring thousands of hours to generate substantial Q_4 silicons. Because of the availability of these data and the simplicity of the isoelectric point, we study below the polymerization of Si(OH)₄ at its isoelectric point in aqueous solutions. This represents our base-case system for developing the new atomic lattice model. We seek a model that agrees with the NMR data on the evolution of the Q_n distribution, while giving atomic-level structural detail lacking in the NMR data. In future work, we will generalize this model to higher pH values relevant for zeolite formation.

Previous atomic-level models of silica provide important information on structure from monomers to rings to clusters. All these models agree on the relatively uniform Si–O bond length of ~ 1.6 Å and the O–Si–O bond angle of $\sim 109^\circ$. Pereira *et al.*^{26,27} applied quantum chemistry to investigate the structures and energetics of various silica chains and rings. They found that four- and six-rings are more stable than five-rings due to their asymmetric arrangement. Garofalini and Martin²⁸ applied molecular dynamics (MD) to study silica polymerization, finding that chains form at early stages followed by ring formation. Rao and Gelb performed large-scale MD simulations of silicic acid in aqueous solution, finding that Ostwald ripening dominates for low silica concentrations at early times; while at longer times, cluster-cluster aggregation is observed. Bhattacharya and Kieffer^{29,30} modeled the sol-gel synthesis of aqueous silica gels, finding three growth regimes: low silica density (0.2 g/cm³) yielded compact nanoparticles, high silica densities (1.0 g/cm³), and low water-to-silicon ratios (denoted as w , $w = 0$) yielded

percolated silica networks, while high densities (1.0 g/cm³) and high water-to-silicon ratios ($w = 5$) led to branched clusters. Despite this progress, none of these MD simulations has reproduced the evolution of the measured Q_n distribution at room temperature, because of the time scale limitations of MD.

To simulate silicic acid polymerization under ambient conditions, Monte Carlo (MC) simulations have been used to overcome the time scale limitations of MD. Wu and Deem³¹ developed a set of cooperative MC moves to study the equilibrium properties of single-cluster growth, finding that silica clusters containing ~ 50 Si atoms are critical nuclei for formation of bulk silica particles. To extend MC simulations to much bigger system sizes, Jorge *et al.*^{16,17} developed a coarse-grained, simple-cubic lattice model to simulate formation of precursor silica-template nanoparticles during early stages of silicalite-1 growth. This model represents each Si(OH)₄ (and its conjugate base) as single particles on the lattice, with first-neighbor attractions accounting for the exothermicity of silicic acid condensation [reaction (1)]. The simple-cubic lattice model accounts for nanoparticle metastability and measured effects of pH and temperature on nanoparticle size. However, the simple-cubic structure precludes pore formation, prompting us to generalize this model to a bcc lattice,¹⁸ which consists of two interpenetrating tetrahedral (diamond) lattices (Fig. 1). By choosing appropriate first-neighbor attractions and second-neighbor repulsions, we found that silica clusters locally populate one sublattice, leaving the empty sublattice as pore space for template molecules. Although this coarse-grained bcc model sheds light on the core-shell structure of silica-template nanoparticles, the coarse-graining makes it impossible to resolve atomic-level details such as Si–O–Si angles and ring-size distributions (RSD).

In the present work, we represent Si and O atoms as distinct particles on the bcc lattice, keeping all Si and O atoms as part of intact SiO₄ tetrahedra. This atomic bcc model of silica represents the simplest possible model that allows for variation in the Si–O–Si angle. We find below that this model gives a rich variety of structures, agrees well with NMR data on the basic kinetics of silica polymerization, and provides quantitative predictions on ring-size distributions in good agreement with analyses of x-ray and neutron diffraction data.

This work is organized as follows. Section II A describes the model and its parameterization and Sec. II B presents the

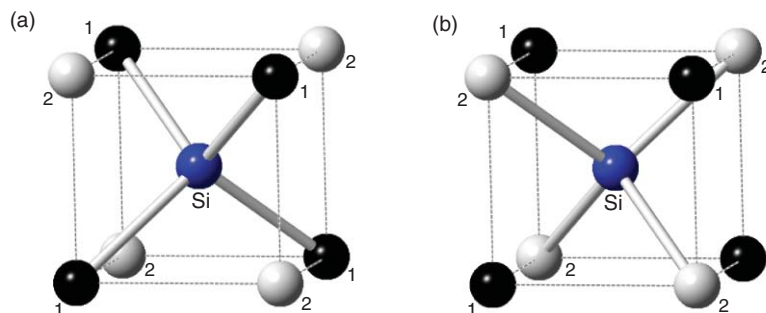


FIG. 1. BCC lattice with black and white spheres denoting sites on two interpenetrating diamond sublattices. The blue sphere in the middle of the cube represents silicon and its four bonding oxygens sit on either (a) black spheres in sublattice 1 or (b) white spheres in sublattice 2.

simulation techniques used in this work. Our main results are presented in Sec. III, and a summary of our results and conclusions is given in Sec. IV.

II. MODEL AND SIMULATION METHODOLOGY

A. Model

The base case of our new model begins by representing $\text{Si}(\text{OH})_4$ molecules as rigid tetrahedra on the bcc lattice. This is accomplished by coarse-graining OH groups into single particles. As such, in our present model each $\text{Si}(\text{OH})_4$ tetrahedron occupies five bcc sites, whereas in our previous bcc model each tetrahedron would occupy only a single site because of the heavier coarse-graining in the previous model.¹⁸ Each $\text{Si}(\text{OH})_4$ unit moves on the lattice via translation and rotation. Because the bcc lattice is equivalent to two interpenetrating diamond sublattices,³² the reorientation move corresponds to switching tetrahedral vertices from one diamond sublattice to the other, as shown in Fig. 1. Water in the system is represented as vacant sites following our previous work.^{16–18} This gives a more plausible coarse-graining than in our previous models, which assumed that $\text{Si}(\text{OH})_4$ and H_2O molecules exclude the same volume. In contrast, our present atomic lattice model assumes that Si atoms, OH groups, and H_2O molecules occupy the same effective volume.

We represent silica condensation—the formation of bridging oxygens as shown in reaction (1)—in our present model by allowing double occupancy of lattice sites by OH groups. This is the only form of double occupancy allowed; i.e., we do not allow a Si atom and an OH group, or two Si atoms, to occupy the same site. The water molecule produced by reaction (1) is represented by the vacancy left behind by the OH group that moved in space, transitioning from single to double occupancy. This double occupancy approach allows the sampling of silica condensation/hydrolysis equilibria while maintaining intact tetrahedra throughout. The energy of double OH occupancy is the exothermicity of silica condensation, represented by $\varepsilon < 0$. The Hamiltonian for this base case model can be written as

$$H = \frac{N\varepsilon}{2} \sum_{n=0}^4 n Q_n, \quad (2)$$

where N is the number of $\text{Si}(\text{OH})_4$ tetrahedra, Q_n is the fraction of Si atoms with n bridging oxygens, and the factor of $1/2$ removes double counting. The parameter ε is determined by fitting model predictions to experimental data on silica solubility.¹ Reduced temperature and all other energy scales are expressed in the units of $|\varepsilon|$. This completes the description of the present base case model.

The atomic bcc model described above allows for Si–O–Si angles of 70° , 109° , and 180° , as shown in Fig. 2. Such angular variation is the key microscopic flexibility allowed by our new lattice model. We note that the 70° angle corresponds to two-rings [Fig. 2(a)], which are generally not observed in silica materials except at very high temperatures³³ because of substantial ring strain. Because we focus on lower temperature sol-gel processing, we discard such two-rings when they arise in random sampling, leaving 109° and 180°

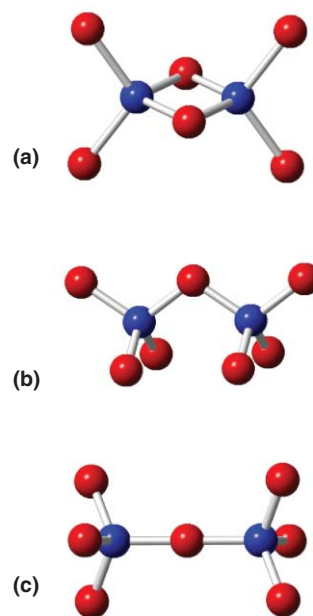


FIG. 2. Possible values of Si–O–Si angle in the base case model: (a) 70° , (b) 109° , and (c) 180° .

as possible Si–O–Si angles. Although these angles are quantitatively different from the range 130° – 180° observed in silica materials,²⁰ our model offers the simplest qualitative treatment of angular variation in network solids. We show below that this model can produce a rich variety of structures of interest in materials science.

Random sampling of the base case model without two-rings produces chalcogenide-like clusters³⁴ dominated by three-rings. Although three-rings have been observed in silica materials by Raman spectroscopy,³⁵ four-rings and larger are more common.¹⁴ Biasing our simulations by penalizing three-ring formation with an energy penalty of $0.6|\varepsilon|$ per three-ring produces exclusively layered clusters dominated by four-rings. Each of the chalcogenide and layered structures is interesting in its own right and will be studied in future work. However, the focus of the present study is on silica materials. We find we can bias the simulation to silica-like structures by penalizing both three- and four-rings with penalties of $\varepsilon_3 = 0.6|\varepsilon|$ and $\varepsilon_4 = 0.3|\varepsilon|$, respectively. The model studied below is thus the base case model without two-rings, and with three- and four-rings penalized according to the following Hamiltonian:

$$H = N_3\varepsilon_3 + N_4\varepsilon_4 + \frac{N\varepsilon}{2} \sum_{n=0}^4 n Q_n, \quad (3)$$

where N_3 and N_4 are the numbers of three- and four-rings, respectively.

For clarity, we now compare our model with the Bell–Salt lattice model,^{36,37} which has been widely used to investigate anomalies of water.^{36–41} The basic idea in the Bell–Salt model is to restrict the coordination number of each molecule to four, and the bonds are tetrahedrally oriented.^{36,37} Like real hydrogen bonds, the bonds are asymmetrical with two “positive” and two “negative” ends. In their model, each

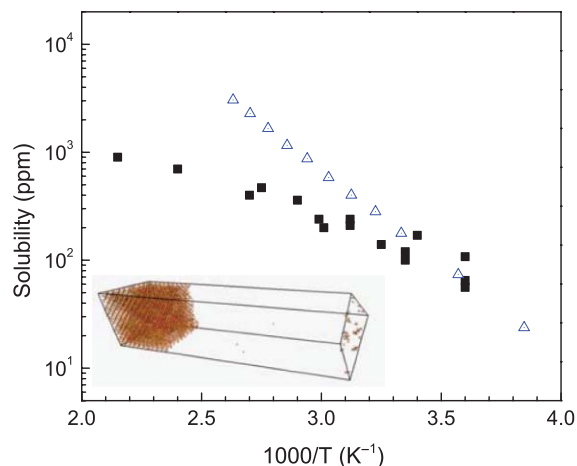


FIG. 3. Solubility of silica at the isoelectric point as a function of temperature. The solid squares represent experimental data from Iler (Ref. 1), and the open triangles show the results of *NVT* simulations. The best fit yields an ϵ value of -4.0 kcal/mol.

molecule is represented by one single site with four bonding directions pointing to the vertices of a tetrahedron. Therefore, each Bell–Salt lattice site is either occupied by a molecule or is vacant. In contrast, our lattice model represents silicon and oxygen atoms of each SiO_4 explicitly, and each $\text{Si}(\text{OH})_4$ unit occupies five sites. As such, each lattice site in our model can be occupied by either one silicon atom, one oxygen atom, or two oxygen atoms. This explicit representation of oxygen atoms enables us to obtain structural information about silica particles such as the evolution of Q_n distributions, morphologies of nanoparticles, and ring-size distributions during silica polymerization.

B. Simulation details

We define the fractional occupancy, x , as the number of tetrahedra divided by the number of bcc sites. For this model, the maximum fractional occupancy is $1/3$, consistent with the formula unit SiO_2 . For reference, the β -cristobalite phase can be represented on our atomic bcc lattice. The density of

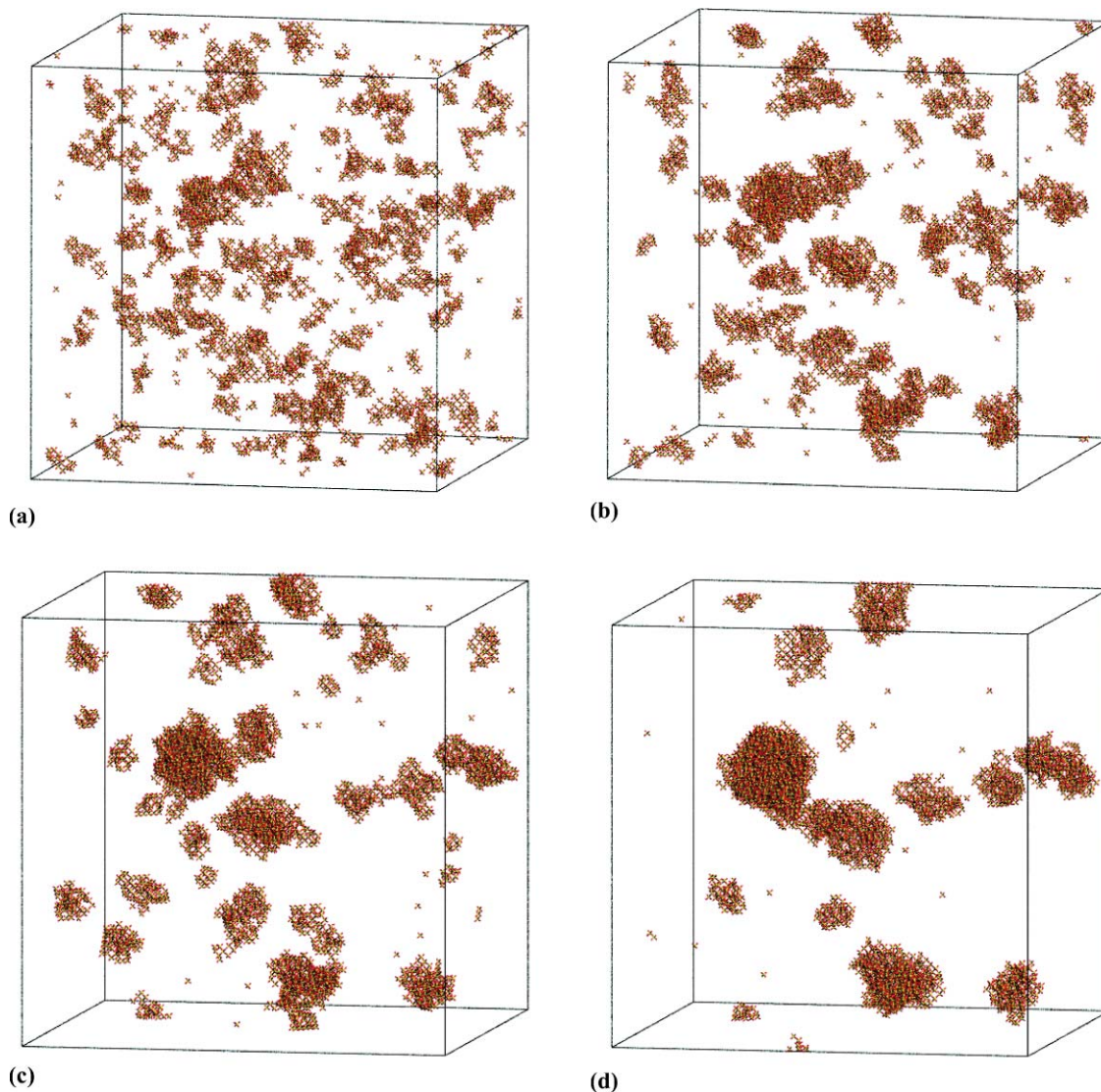


FIG. 4. Simulation snapshots of silica polymerization with a mole fraction of $x = 0.002$ and room temperature (reduced temperature $T^* = 0.15$). Snapshots are taken at (a) 10^4 , (b) 10^5 , (c) 5×10^5 , and (d) 5×10^6 MC steps. Snapshots are generated using Visual Molecular Dynamics (Ref. 50).

β -cristobalite is 2.3 g/cm^3 ,¹ corresponding to a fractional occupancy of $x = 0.0625$ on our lattice. We simulated polymerization at two silica concentrations: a fractional occupancy of $x = 0.002$ corresponding to a silica concentration of 0.074 g/cm^3 and an occupancy of $x = 0.02732$ corresponding to a concentration of 1.0 g/cm^3 . The lower concentration corresponds to that encountered in the clear-solution synthesis of silicalite-1 at room temperature,^{42,43} although in our case we have no structure-directing agent. The higher concentration corresponds to the system studied by Devreux *et al.*,¹² who performed NMR measurements of the evolution of silica Q_n distributions. The number of bcc sites is $2L^3$, where L is the simulation cell edge length in units of the bcc lattice parameter, and the factor of 2 counts the two sites per bcc unit cell. We used $L = 100$ and 60 for the low and high concentrations, respectively, corresponding to 4000 and 11 802 tetrahedra. We have found that simulation cells with $L = 60, 80$, and 100 give essentially identical Q_n distributions and ring-size distributions, indicating negligible system size effects.

We performed MC simulations in the canonical ensemble, initiated with silica monomers randomly distributed on a

bcc lattice with periodic boundary conditions. Two kinds of moves were attempted in the simulations: rotations and translations of silica tetrahedra. For a given tetrahedron, a rotation was carried out by switching its vertices (oxygen atoms) from one diamond sublattice to the other, as shown in Fig. 1. Translations were attempted by moving a given tetrahedron to any location in the simulation cell, a form of Glauber dynamics. Moves were automatically rejected, if they produce multiple site occupancy, with the notable exception of allowed double OH occupancies. Moves that produced allowed occupancies were then accepted or rejected with the usual Metropolis criterion, using the Hamiltonian in Eq. (3) to compute energy differences. One MC “step” consists of N attempted translations and N attempted rotations, where N is the number of silica tetrahedra in the simulation. We note that, although the total number of bcc sites occupied by silicon and oxygen atoms varies as two vertices from adjacent tetrahedra may occupy the same site, the number of tetrahedra remained constant during our simulations. We kept track of clusters formed during simulations via the Hoshen–Kopelman cluster counting algorithm.⁴⁴

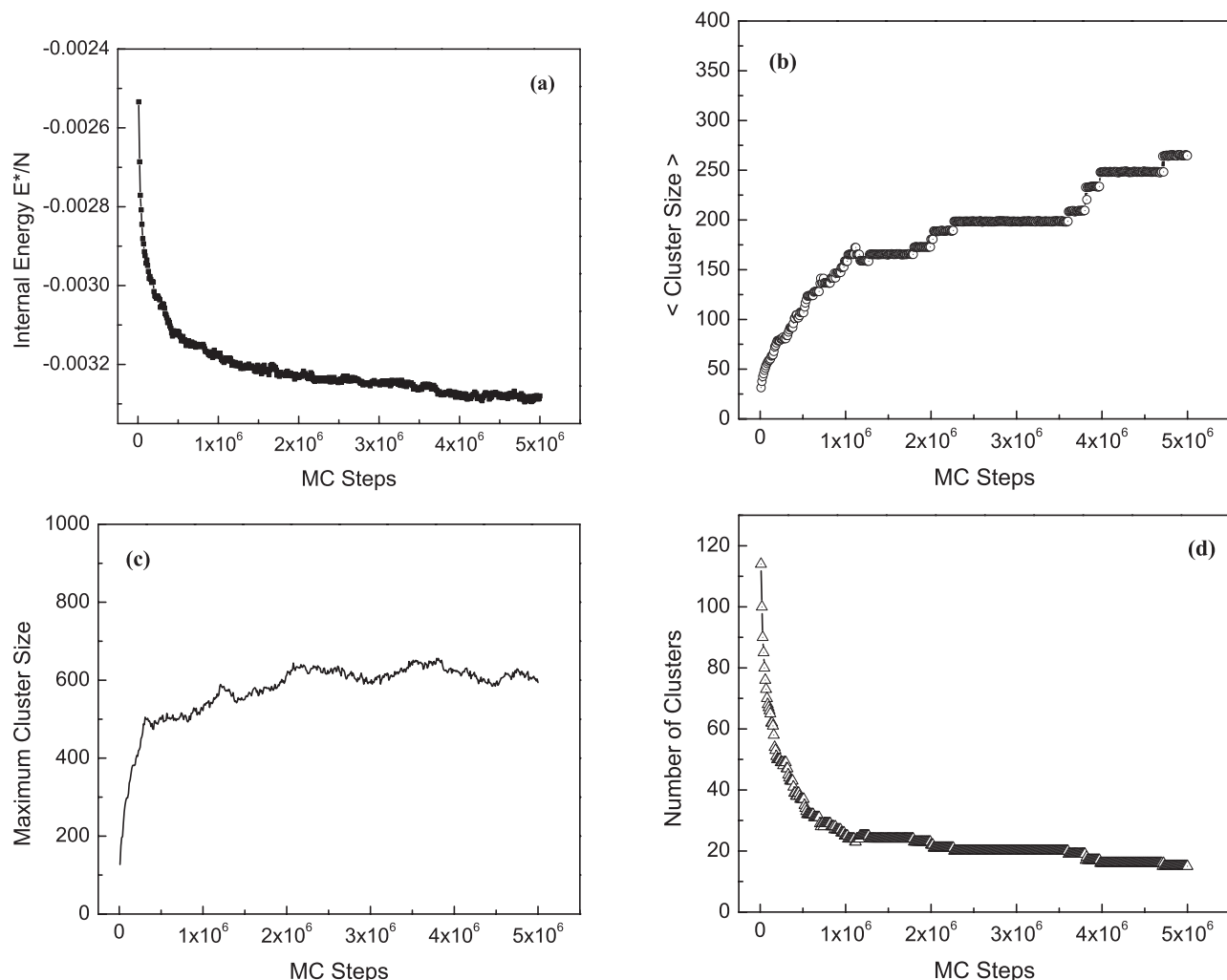


FIG. 5. Energy and cluster evolution for $x = 0.002$ and $T^* = 0.15$. (a) Reduced energy of system per lattice site, (b) average cluster size, (c) maximum cluster size, and (d) total number of clusters.

III. RESULTS AND DISCUSSION

We begin by calibrating the silica condensation energy, ε , given in Eqs. (2) and (3). The procedure is described in detail in previous works.^{16,18} In brief, we performed canonical MC simulations initialized with a slab of β -cristobalite, in contact with pure solvent (i.e., vacancies) with periodic boundaries in the directions perpendicular to the slab surface, as shown in Fig. 3. We then simulated silica solubility for comparison with experimental values.¹ The best fit is obtained with a ε value of -4.0 kcal/mol, in good agreement with the calculated condensation energy (-3.2 kcal/mol) for dimer formation from two $\text{Si}(\text{OH})_4$ molecules, obtained from density functional theory coupled with a continuum dielectric model.^{45,46} The difference between the experimental and simulated solubilities comes from various approximations in the lattice model, which remains rather simple compared to forcefield-based approaches. In particular, there is only one tunable parameter—the silica condensation energy—which limits the flexibility of the model for describing the temperature dependence of the solubility. We chose the condensation energy value that produces good agreement for the solubility at 25°C . Reduced temperatures are thus defined as $T^* = kT/|\varepsilon|$, with room temperature corresponding to $T^* = 0.15$.

A. Lower concentration system

A series of snapshots from the lower concentration system at $T^* = 0.15$ is shown in Fig. 4. After about 10^4 MC steps, the system evolved from a configuration with many smaller clusters to one with fewer larger ones. The evolution of energy and cluster size during MC is shown in Fig. 5. The simulated behavior is qualitatively similar to that seen in our more coarse-grained models of silica polymerization.^{16–18} In particular, the energy is seen to decrease dramatically until about 5×10^5 MC steps, and then to continue decreasing more slowly thereafter. The average cluster size increases rapidly until about 10^6 MC steps, with small step-wise jumps in cluster size thereafter. The maximum cluster size shows a rapid increase to 500 tetrahedra by 2×10^5 MC steps, followed by fluctuations around 600 tetrahedra thereafter. The evolution of the number of clusters mirrors that in the average cluster size because of the fixed number of tetrahedra in the simulation.

The simulated evolution of the Q_n distribution is shown in Fig. 6 versus the number of MC steps and also versus the degree of condensation defined by $c = \sum_{n=0}^4 nQ_n/4$. We note that the degree of condensation, which is the fraction of terminal oxygens converted to bridging oxygens, is proportional to our model energy according to $E = 2N\varepsilon c$. As expected, Q_0 silica is rapidly consumed as monomers form dimers, oligomers, and silica particles. The evolution of Q_1 shows a peak at around 10^2 MC steps, followed by a peak in Q_2 at around 10^3 MC steps. The peak in Q_3 appears much later, at $\sim 5 \times 10^4$ steps. The degree of condensation, c , reaches a value around 0.86 after 5×10^6 MC steps. This is a high degree of polymerization compared with

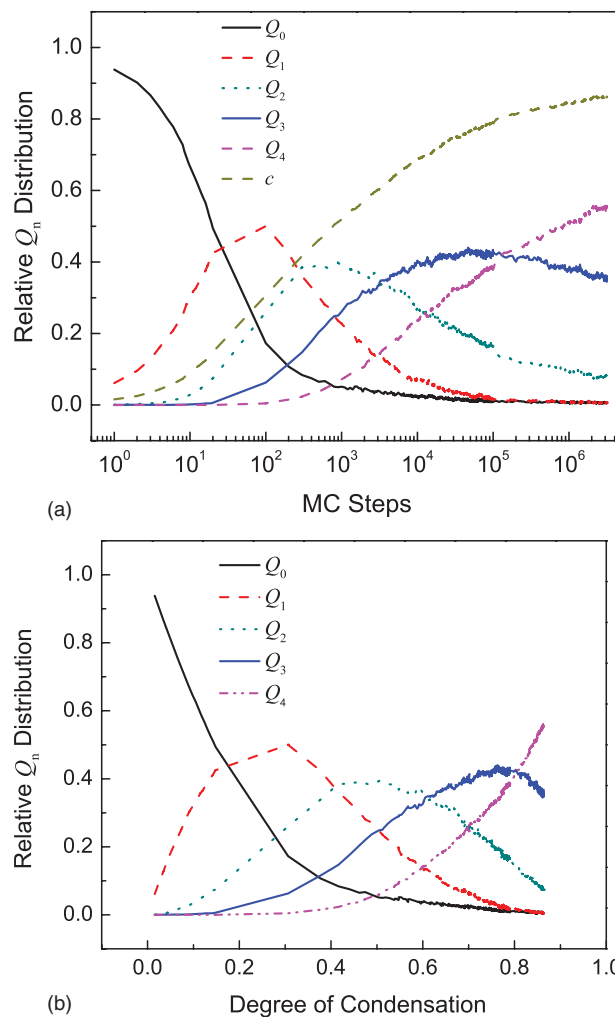


FIG. 6. Q_n distributions for $x = 0.002$ and $T^* = 0.15$, as a function of (a) logarithm of MC simulation steps, (b) degree of condensation defined as $c = \sum_{n=0}^4 nQ_n/4$.

other simulation studies, and is comparable to that seen experimentally for higher silica concentrations.⁴⁷

The evolution of the Q_n distribution provides important information about the polymerization mechanism. We note that Q_0 counts only monomers, Q_1 reflects dimers and terminal $\equiv\text{Si}-\text{OH}$ groups, Q_2 represents both linear and cyclic chains, and Q_3 and Q_4 indicate the formation of three-dimensional network structures. The connection between the Q_n distribution and molecular structure can be seen in Fig. 7 which shows magnified ($6.5\times$) simulation snapshots at simulation times associated with the maxima in Q_1 , Q_2 , and Q_3 , respectively. Figure 7(a) shows a solution of dimers, Fig. 7(b) displays longer noncyclic chains, and Fig. 7(c) shows the formation of compact nanoparticles with high degrees of condensation.

It is thought that during the early stages of silica polymerization, Ostwald ripening plays an important role in the process.¹ This is driven by the enhanced solubility of silica in smaller particles because of the larger surface-to-volume ratios in such clusters. Ostwald ripening is indeed the mechanism that controls cluster growth in the present

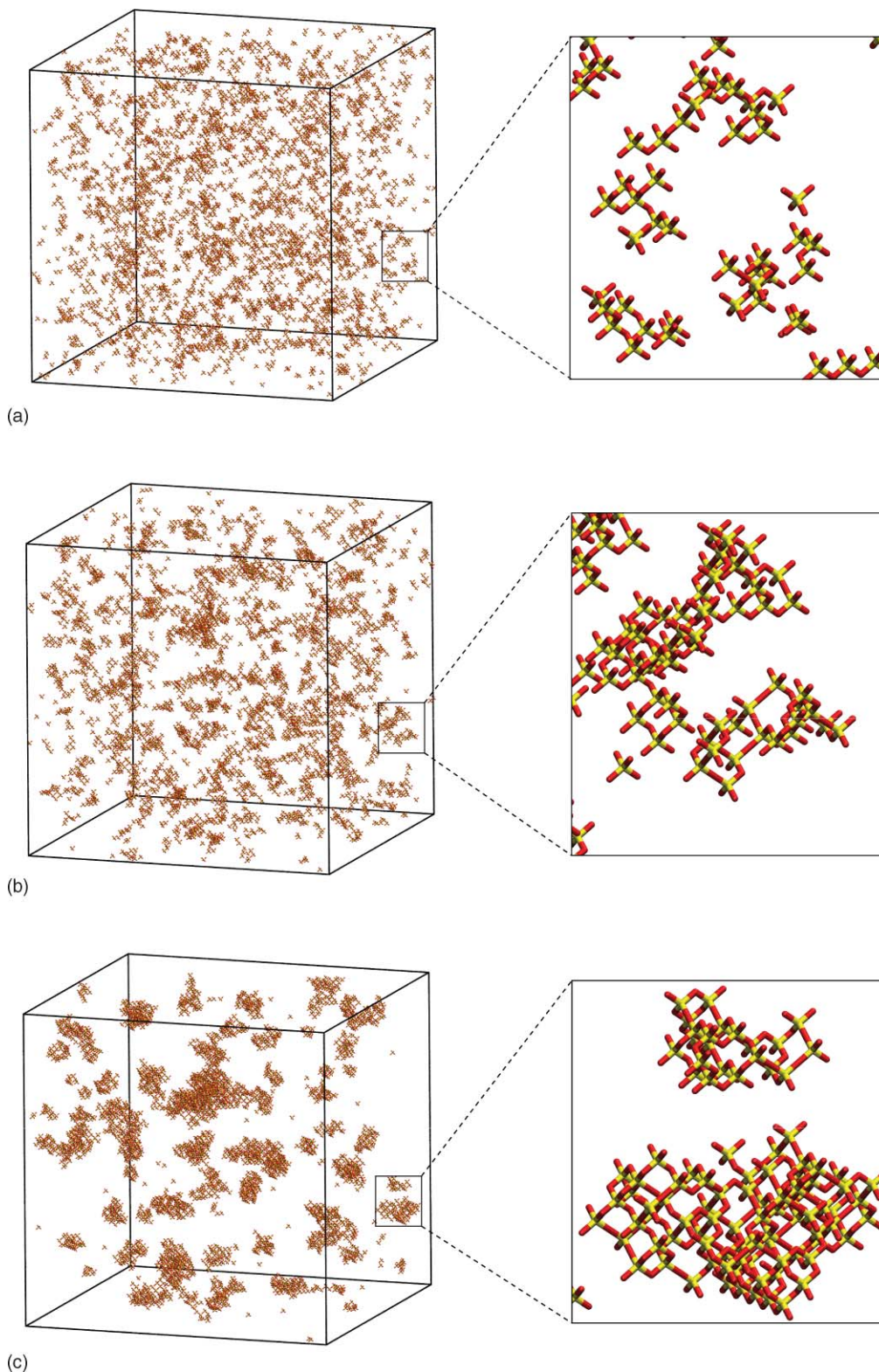


FIG. 7. Magnified ($6.5\times$) snapshots taken from $x = 0.002$ and $T^* = 0.15$ at (a) 10^2 MC steps, (b) 10^3 MC steps, and (c) 5×10^4 MC steps, corresponding to peaks of Q_1 , Q_2 , and Q_3 in Fig. 6, respectively.

simulations, precisely because we do not include overall cluster moves in the MC that would promote the competing mechanism of cluster–cluster aggregation. Nonetheless, when two clusters are sufficiently close, they have exhibited coalescence phenomena as exemplified in Fig. 8. In this

case only 5×10^3 MC steps were required to bridge the two particles, but another 4×10^5 steps were required to thicken the neck, essentially completing the coalescence.

We now discuss the evolution of the ring-size distribution at $T^* = 0.15$ and $x = 0.002$, shown in Fig. 9. The ring

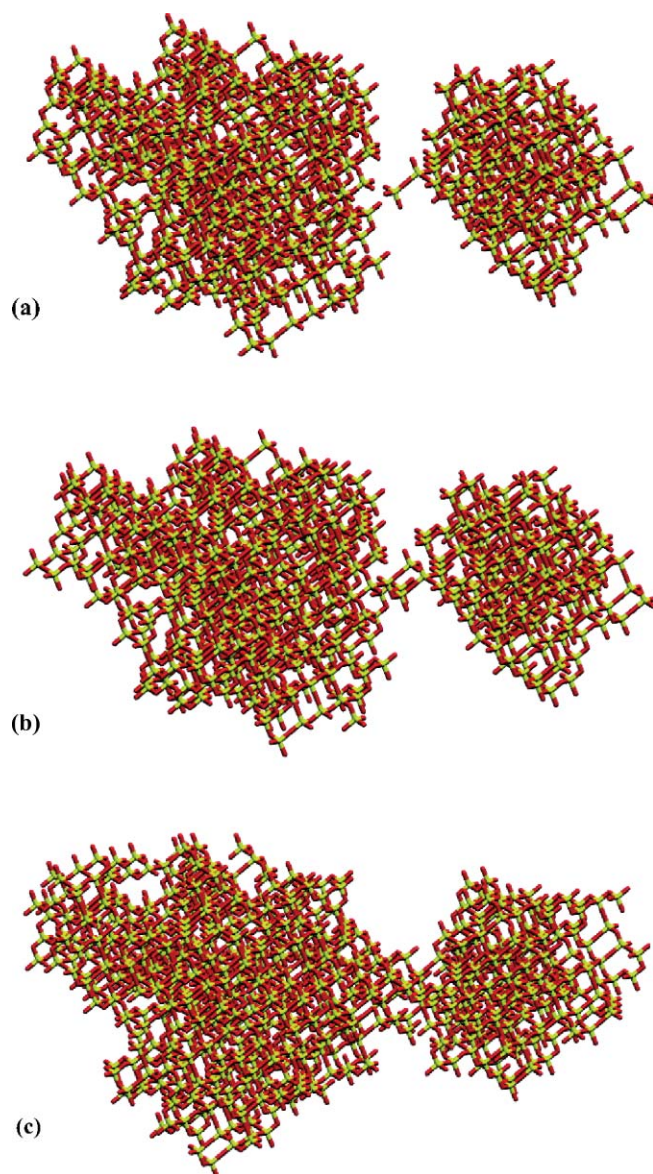


FIG. 8. Coalescence between two silica particles during an NVT MC simulation at $T^* = 0.15$ and $x = 0.002$. (a) At 3.8×10^5 MC steps, the silica particles on the left and right contain 463 and 200 $\text{Si}(\text{OH})_4$ tetrahedra, respectively, (b) at 3.85×10^5 MC steps the silica particle contains 675 $\text{Si}(\text{OH})_4$ units, and (c) at 7.5×10^5 MC steps the silica particle contains 790 $\text{Si}(\text{OH})_4$ units.

counting algorithm⁴⁸ we have used detects fundamental rings, defined as rings that cannot be divided into two smaller rings. We performed three statistically independent MC simulations to obtain the RSD, shown in Fig. 9 with standard deviations shown as error bars. As the simulation proceeds, both average ring size and the number of rings increase. At around 10^3 MC steps three-rings start to form, coinciding with Q_2 reaching its maximum value and an overall degree of condensation of 0.5. After about 10^4 steps, four-rings become the most common with the number of three-rings decreasing slightly, and rings as large as ten-rings beginning to emerge. After about 10^5 steps, six- and eight-rings become the most common followed by five- and seven-rings. As silica polymerization proceeds, larger rings (up to 15-rings) are observed with increasing frequency. Compared with RSDs of known zeolites and

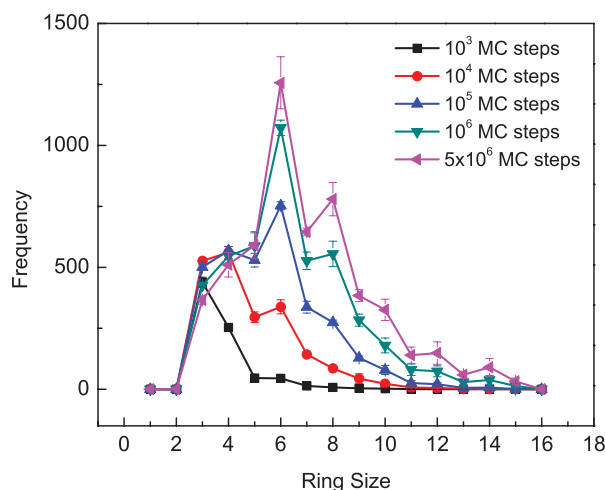


FIG. 9. Ring-size distributions for $T^* = 0.15$ and $x = 0.002$ at the following stages of MC: 10^3 , 10^4 , 10^5 , 10^6 , and 5×10^6 MC steps.

results from previous simulations of amorphous silica,^{31,49} the final RSD in Fig. 9 is in reasonable agreement, with significant population of 3- to 12-rings, and dominance of 6- and 8-rings. Our results are also in qualitative agreement with quantum calculations^{26,27} which find that six-rings are more stable than five-rings, but larger rings were not considered.

B. Higher concentration system

The simulations on the higher concentration system allow closer contact with experiment. First we compare experiment and simulation of the Q_n distribution as a function of the degree of condensation, c , as shown in Fig. 10. In general, the agreement is quite good, especially given the simplicity of the model. The locations of the simulated Q_1 , Q_2 , and Q_3 peaks are in excellent agreement with experiment, at c values of 0.25, 0.5, and 0.8, respectively. On the other hand, the heights of these simulated peaks are lower than experimental values, especially for Q_2 . This is mostly because of the early onset of Q_4 silica in our simulations, a likely consequence of using the lattice model.

Although the MC simulation lacks a system clock, we can still compare the temporal evolution of experimental Q_n distributions with simulation “stage” measured by the number of MC steps. This is shown in Fig. 11, where the two graphs are aligned by the Q_0/Q_1 crossing point. We see in Fig. 11 that the peaks in Q_1 , Q_2 , and Q_3 are in good agreement between experimental time and simulation steps. This indicates a roughly linear relationship between MC step and physical time that persists for over three orders of magnitude for both. Using the Q_2 peak (2 h or 30 MC steps) to determine the proportionality constant indicates that each MC step corresponds to 4 min of physical time. We can also use the Q_n crossing points in Fig. 11 to assess agreement between experiment and simulation. Although the Q_1/Q_2 crossing point occurs to the right (i.e., “later”) than that in experiment, the simulated Q_3/Q_4 crossing point occurs well before experiment; indeed, this crossing point is not observed in the 6000 h experimental time window. As such, the simulated polymerization process

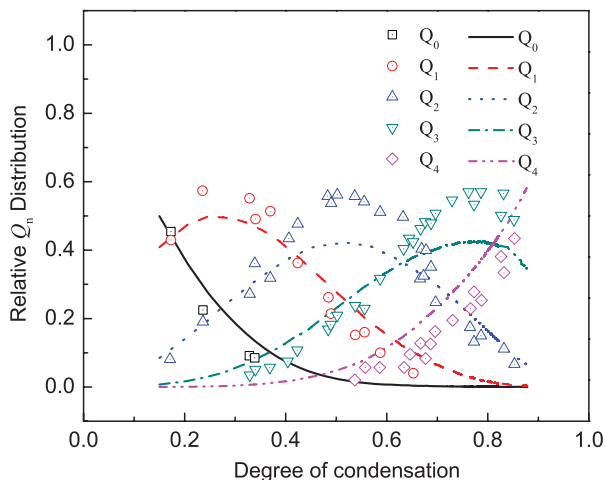


FIG. 10. Q_n distribution for $T^* = 0.15$ and $x = 0.02732$ as a function of the degree of condensation c . Symbols are experimental results from NMR studies (Ref. 12), \square , \circ , \triangle , ∇ and \diamond represent measured Q_0 , Q_1 , Q_2 , Q_3 , and Q_4 data. Solid line, dashed line, dotted line, dashed-dotted line, and dashed-dotted-dotted line give simulated Q_n results.

is clearly accelerated compared to experiment, likely from the use of Glauber MC dynamics which ignore diffusion limitations. In addition, the lattice model itself likely facilitates Q_4 formation through the existence of ready-made coordination geometries. Nonetheless, this lattice model has allowed much larger system sizes compared to previous atomistic models. In addition, our model has produced much greater degrees of condensation at room temperature, shedding light on structural properties, such as RSDs, which we now discuss for the high concentration system.

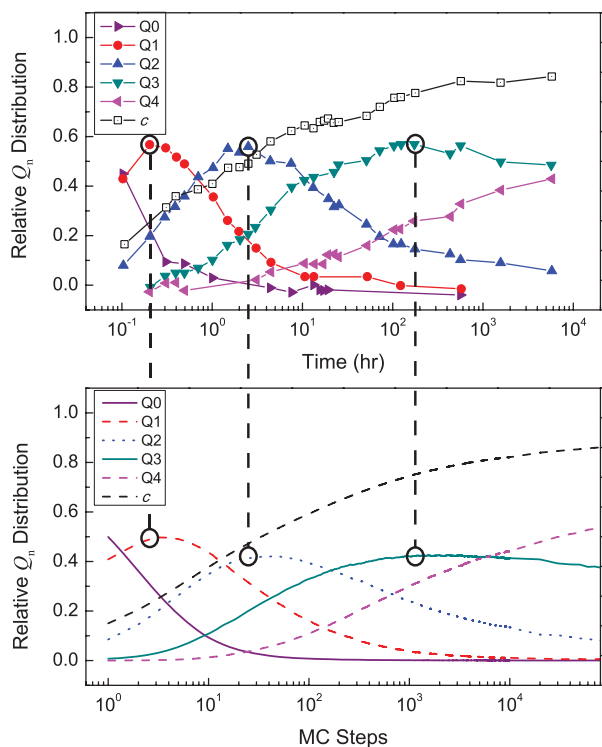


FIG. 11. (a) Q_n distributions extracted from experimental results (Ref. 12). (b) Simulated Q_n distributions at $x = 0.02732$ and $T^* = 0.15$.

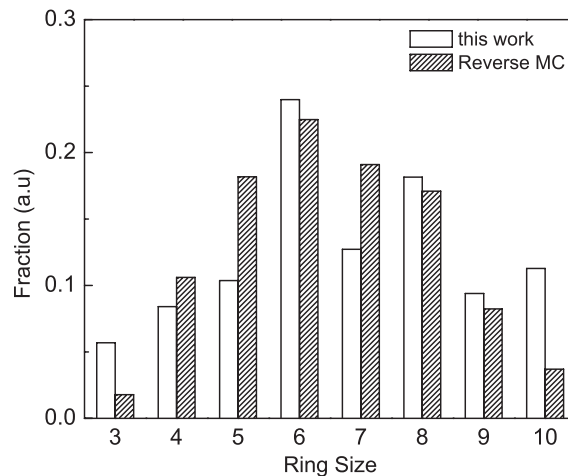


FIG. 12. Comparison of simulated RSD at $x = 0.02732$ and $T^* = 0.15$ with reverse Monte Carlo analysis of neutron and x-ray diffraction from vitreous silica in Ref. 14. Both simulation and reverse Monte Carlo agree on the dominance of six-rings in amorphous silica.

Kohara and Suzuya¹⁴ obtained RSDs for vitreous silica and germania by interpreting high energy x-ray and neutron diffraction measurements via reverse Monte Carlo. Their results for the RSD of vitreous silica are essentially the only experimental data available to test our predictions on dense, amorphous silica. In Fig. 12 we compare our simulated high

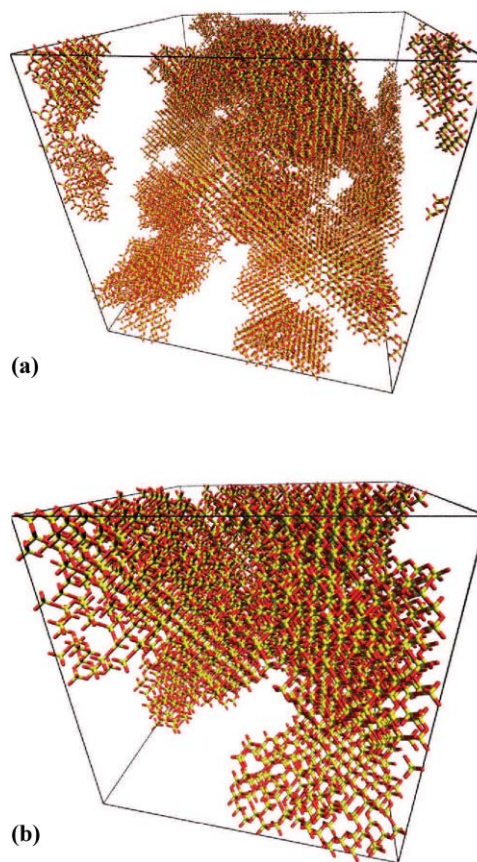


FIG. 13. (a) Snapshot from MC simulation at $x = 0.02732$ and $T^* = 0.15$, the same conditions as in Fig. 10. (b) Magnified ($2\times$) snapshot showing enhanced branching and cross-linking predicted in silica at higher concentration.

concentration RSD with that of Kohara and Suzuya, focusing on the range of three- to ten-rings in their work. The overall agreement is very good. Our simulations are dominated by six- and eight-rings (as they are at lower concentration), with seven- and ten-rings also prominent. The results of Kohara and Suzuya are dominated by six-rings, with five-, seven- and eight-rings playing major roles as well. Simulation and experiment agree in the predominance of six-rings, consistent with quantum calculations on ring stability.^{26,27} On the other hand, experiment suggests that five- and seven-rings are important, while simulation predicts that three- and ten-rings are frequent. This discrepancy is likely caused by the use of a lattice model.

Figure 13 shows snapshots from the simulation at higher concentration. The higher concentration makes it difficult to see structural details clearly at this length scale. A magnified view of one corner of the system is shown in Fig. 13(b). The silica structures formed under these conditions exhibit much more branching and cross-linking, as noted by Bhattacharya and Kieffer based on MD simulations.^{29,30}

IV. SUMMARY AND CONCLUSIONS

We have presented a new atomic lattice model for silica polymerization building on earlier work.^{16–18} The present model involves Si and O atoms occupying the sites of a bcc lattice, with all atoms arranged in rigid SiO₄ tetrahedra. This model allows for variation in the Si–O–Si angle, giving possible values of 109° and 180°. We have enforced restrictions on the formation of two-rings by discarding them, and on three- and four-rings through energy penalties. This model allows for a more detailed structural study of silica polymerization than was possible with previous lattice models,^{16–18} while allowing the study of larger system sizes than in earlier atomistic models.^{28,31,49} Through suitable choices of energy penalties on rings, this model can also shed light on structure formation in related materials—chalcogenides and layered materials.

We have studied two conditions for silica assembly, both at room temperature and the isoelectric pH of silica: a lower silica concentration relevant to the clear solution synthesis of zeolite silicalite-1, and a higher concentration corresponding to NMR measurements of the Q_n distribution. Our simulations suggest that silica polymerization proceeds as follows: (a) dimer and small oligomer formation, (b) growth of non-cyclic chains, (c) ring formation and growth of spherical particles, (d) Ostwald ripening of larger particles at the expense of smaller ones, and (e) cross-linking between particles for systems with high silica concentrations. The simulated Q_n evolution is in very good agreement with the NMR data for the high concentration system. In particular, three-dimensional network formation is found to be very slow, requiring an order of magnitude in time and Monte Carlo steps to proceed from Q_1 to Q_2 structures, and another order of magnitude in time and Monte Carlo steps to go from Q_2 to Q_3 . Our lattice model simulations do exhibit a tendency to accelerate formation of more compact, Q_3 and Q_4 silica. Our simulations show the evolution of rings, from 3- and 4-rings formed at early times, to rings as large as 15-rings at later times. The dominance of

six-rings in our simulations is consistent with quantum calculations of ring stability, and also with reverse Monte Carlo analyses of x-ray and neutron diffraction from vitreous silica.

The simplicity of the present model together with its computational efficiency could make it a valuable tool in understanding the self-assembly of silica materials and other closely related systems. In the future, we will apply this model to silica at higher pH values relevant to zeolite formation.

ACKNOWLEDGMENTS

This work was supported by a grant from the U. S. Department of Energy (Contract No. DE-FG02-07ER46466). The authors thank Professor J. Machta for advice on Monte Carlo methods.

- ¹R. K. Iler, *The Chemistry of Silica: Solubility, Polymerization, Colloid and Surface Properties and Biochemistry* (Wiley, New York, 1979).
- ²C. J. Brinker and G. W. Scherer, *Sol-Gel Science: The Physics and Chemistry of Sol-Gel Processing* (Academic, New York, 1989).
- ³L. L. Hench and J. K. West, *Chem. Rev.* **90**, 33 (1990).
- ⁴E. I. Halasz, *Silica and Silicates in Modern Catalysis* (Transworld Research Network, Kerala, 2010).
- ⁵S. M. Auerbach, K. A. Carrado, and P. K. Dutta, *Handbook of Zeolite Science and Technology* (Marcel Dekker, New York, 2003).
- ⁶C. T. Kresge, M. E. Leonowicz, W. J. Roth, J. C. Vartuli, and J. S. Beck, *Nature (London)* **359**, 710 (1992).
- ⁷H. Dislich and P. Hinz, *J. Non-Cryst. Solids* **48**, 11 (1982).
- ⁸H. Dislich, *J. Non-Cryst. Solids* **57**, 371 (1983).
- ⁹R. W. Schwartz, T. Schneller, and R. Waser, *C. R. Chim* **7**, 433 (2004).
- ¹⁰T. J. Barton, L. M. Bull, W. G. Klemperer, D. A. Loy, B. McEnaney, M. Misono, P. A. Monson, G. Pez, G. W. Scherer, J. C. Vartuli, and O. M. Yaghi, *Chem. Mater.* **11**, 2633 (1999).
- ¹¹R. A. Assink and B. D. Kay, *J. Non-Cryst. Solids* **99**, 359 (1988).
- ¹²F. Devreux, J. P. Boilot, F. Chaput, and A. Lecomte, *Phys. Rev. A* **41**, 6901 (1990).
- ¹³R. A. Assink and B. D. Kay, *Annu. Rev. Mater. Sci.* **21**, 491 (1991).
- ¹⁴S. Kohara and K. Suzuya, *J. Phys.: Condens. Matter* **17**, S77 (2005).
- ¹⁵S. M. Auerbach, M. H. Ford, and P. A. Monson, *Curr. Opin. Colloid Interface Sci.* **10**, 220 (2005).
- ¹⁶M. Jorge, S. M. Auerbach, and P. A. Monson, *J. Am. Chem. Soc.* **127**, 14388 (2005).
- ¹⁷M. Jorge, S. M. Auerbach, and P. A. Monson, *Mol. Phys.* **104**, 3513 (2006).
- ¹⁸L. Jin, S. M. Auerbach, and P. A. Monson, *J. Phys. Chem. C* **114**, 14393 (2010).
- ¹⁹A. Malani, S. M. Auerbach, and P. A. Monson, *J. Phys. Chem. Lett.* **1**, 3219 (2010).
- ²⁰W. H. Baur, *Acta Crystallogr.* **36**, 2198 (1980).
- ²¹I. Petrovic, A. Navrotsky, M. E. Davis, and S. I. Zones, *Chem. Mater.* **5**, 1805 (1993).
- ²²P. M. Piccione, C. Laberty, S. Y. Yang, M. A. Cambor, A. Navrotsky, and M. E. Davis, *J. Phys. Chem. B* **104**, 10001 (2000).
- ²³R. G. Larson, *J. Chem. Phys.* **91**, 2479 (1989).
- ²⁴F. R. Siperstein and K. E. Gubbins, *Langmuir* **19**, 2049 (2003).
- ²⁵G. A. Parks, *Chem. Rev.* **65**, 177 (1965).
- ²⁶J. C. G. Pereira, C. R. A. Catlow, and G. D. Price, *J. Phys. Chem. A* **103**, 3252 (1999a).
- ²⁷J. C. G. Pereira, C. R. A. Catlow, and G. D. Price, *J. Phys. Chem. A* **103**, 3268 (1999b).
- ²⁸S. H. Garofalini and G. Martin, *J. Phys. Chem.* **98**, 1311 (1994).
- ²⁹S. Bhattacharya and J. Kieffer, *J. Chem. Phys.* **122**, 094715 (2005).
- ³⁰S. Bhattacharya and J. Kieffer, *J. Phys. Chem. C* **112**, 1764 (2008).
- ³¹M. G. Wu and M. W. Deem, *J. Chem. Phys.* **116**, 2125 (2002).
- ³²C. Kittel, *Introduction to Solid State Physics* (Wiley, New York, 1996).
- ³³C. A. Demmelmaier, R. E. White, J. A. van Bokhoven, and S. L. Scott, *J. Catal.* **262**, 44 (2009).
- ³⁴N. Zheng, X. Bu, B. Wang, and P. Feng, *Science* **298**, 2366 (2002).

- ³⁵H. Fan, C. Hartshorn, T. Buchheit, D. Tallant, R. Assink, R. Simpson, D. J. Kisse, D. J. Lacks, S. Torquato, and C. J. Brinker, *Nature Mater.* **6**, 418 (2007).
- ³⁶G. M. Bell, *J. Phys. C* **5**, 889 (1972).
- ³⁷G. M. Bell and D. W. Salt, *J. Chem. Soc., Faraday Trans. 2* **72**, 76 (1976).
- ³⁸D. A. Lavis and B. W. Southern, *J. Stat. Phys.* **35**, 489 (1984).
- ³⁹S. S. Borick and P. G. Debenedetti, *J. Phys. Chem.* **97**, 6292 (1993).
- ⁴⁰S. S. Borick, P. G. Debenedetti, and S. Sastry, *J. Phys. Chem.* **99**, 3781 (1995).
- ⁴¹J.-C. Liu, P. A. Monson, and F. van Swol, *J. Phys. Chem. C* **111**, 15976 (2007).
- ⁴²J. M. Fedeyko, J. D. Rimer, R. F. Lobo, and D. G. Vlachos, *J. Phys. Chem. B* **108**, 12271 (2004).
- ⁴³T. M. Davis, T. O. Drews, H. Ramanan, C. He, J. S. Dong, H. Schnablegger, M. A. Katsoulakis, E. Kokkoli, A. V. McCormick, R. L. Penn, and M. Tsapatsis, *Nature Mater.* **5**, 400 (2006).
- ⁴⁴J. Hoshen and R. Kopelman, *Phys. Rev. B* **14**, 3438 (1976).
- ⁴⁵C. R. A. Catlow, L. Ackermann, R. G. Bell, F. Cora, D. H. Gay, M. A. Nygren, J. C. Pereira, G. Sastre, B. Slater, and P. E. Sinclair, *Faraday Discuss.* **106**, 1 (1997).
- ⁴⁶J. C. G. Pereira, C. R. A. Catlow, and G. D. Price, *Chem. Commun. (Cambridge)* **1998**, 1387.
- ⁴⁷L. Malier, J. P. Boilot, F. Chaput, and F. Devreus, *Phys. Rev. A* **46**, 959 (1992).
- ⁴⁸X. L. Yuan and A. N. Cormack, *Comput. Mater. Sci.* **24**, 343 (2002).
- ⁴⁹N. Z. Rao and L. D. Gelb, *J. Phys. Chem. B* **108**, 12418 (2004).
- ⁵⁰W. Humphrey, A. Dalke, and K. Schulten, *J. Mol. Graphics* **14**, 33 (1996).